

Cavity QED treatment of scattering-induced efficient free-space excitation and collection in high-Q whispering-gallery microcavities

Yong-Chun Liu, Yun-Feng Xiao,* Xue-Feng Jiang, Bei-Bei Li, Yan Li, and Qihuang Gong†

*State Key Lab for Mesoscopic Physics, School of Physics,
Peking University, Beijing 100871, People's Republic of China
(Dated: March 8, 2013)*

Whispering-gallery microcavity laser possesses ultralow threshold, whereas convenient free-space optical excitation and collection suffer from low efficiencies due to its rotational symmetry. Here we analytically study a three-dimensional microsphere coupled to a nano-sized scatterer in the framework of quantum optics. It is found that the scatterer is capable of coupling light in and out of the whispering-gallery modes (WGMs) without seriously degrading their high-Q properties, while the microsphere itself plays the role of a lens to focus the input beam on the scatterer and vice versa. Our analytical results show that (1) the high-Q WGMs can be excited in free space, and (2) over 50% of the microcavity laser emission can be collected within less than 1° . This coupling system holds great potential for low threshold microlasers free of external couplers.

PACS numbers: 42.60.Da, 42.55.Sa, 42.50.Ct

I. INTRODUCTION

Whispering-gallery mode (WGM) microcavities represent one of the most promising candidates for a wide range of fundamental studies and applications, including cavity quantum electrodynamics, cavity optomechanics, microlasers, filters and biological sensors (for reviews, see [1–4]). Unfortunately, due to the rotational symmetry, they suffer from inefficient coupling with the outside modes, which limits their applications, especially in microlasers [5]. One of the solutions is the tapered fiber coupling method [6–8], which possesses nearly unity efficiency. Nevertheless, convenient free-space coupling without near-field couplers is eagerly required because of the experimental limitations [9–11]. For example, the external couplers are not convenient at low temperature chambers; for a higher-index-material resonator [12, 13], its coupling with the tapered fiber is inefficient due to the phase mismatch. Alternatively, deformed cavities (also named as asymmetric resonant cavity, ARC) are proposed [14–30], because they allow high-efficiency free-space excitation and directional emission. Latest developments in ARC studies include Limacon-shaped cavity [31–34] and circular disk cavity with a linear [35] or point defect in it [36, 37], but the emission divergence angles are still too broad. Very recently, highly directional outputs are obtained in an elliptical microdisk with a notch at the boundary [38], and by placing a nanoparticle into the evanescent wave region of microcavities [39]. These investigations focused on two-dimensional (2D) microcavity systems by resorting to numerical simulations.

However, 2D microcavities exhibit relatively low quality (Q) factors in experiment and there are significant energy losses in the perpendicular dimension. Thus, there is an interest to employ 3D microcavities, whereas it is difficult to perform numerical simulations. Here we present a cavity quantum electrodynamics (QED) treatment of 3D microsphere-scatterer coupling system, and derive analytical expression of the free-space excitation and the emission directionality. Our results explicitly reveal the underlying physics and is also suitable for 2D case.

The paper is organized as follows. In Sec II, we briefly describe the microsphere-scatterer coupling system. In Sec. III and IV, we investigate the free-space excitation of WGMs and free-space collection of scattered lasing modes, respectively. Conclusions are presented in Sec. IV.

II. SCATTERER-MICROSPHERE SYSTEM

Figure 1(a) illustrates a schematic of the present system. A spherical subwavelength scatterer (radius r_s) locates on the surface of a microsphere (radius R) which is doped with gain medium for the microlaser applications. A Gaussian pump laser beam (vacuum wavelength λ_1 , satisfying $r_s \ll \lambda_1 \ll R$) with the polarization in x axis direction propagates along $-z$ axis, and is incident to the microsphere. Here we have established the Cartesian and spherical coordinate systems with the scatterer located at the origin O , as sketched in the bottom left of Fig. 1(a). The subwavelength scatterer can be treated as a dipole [40, 41], with the dipole moment induced by the electric fields of the input Gaussian modes, the excitation and lasing WGMs and the reservoir modes in the free space. The Rayleigh scattering results in the interaction among these modes, by which the input photons are scattered into the excitation WGMs, and the lasing photons in WGMs are scattered into the reservoir modes.

*To whom correspondence should be addressed.
Electronic address: yfxiao@pku.edu.cn.
URL: www.phy.pku.edu.cn/~yfxiao/index.html
†Electronic address: qhgong@pku.edu.cn

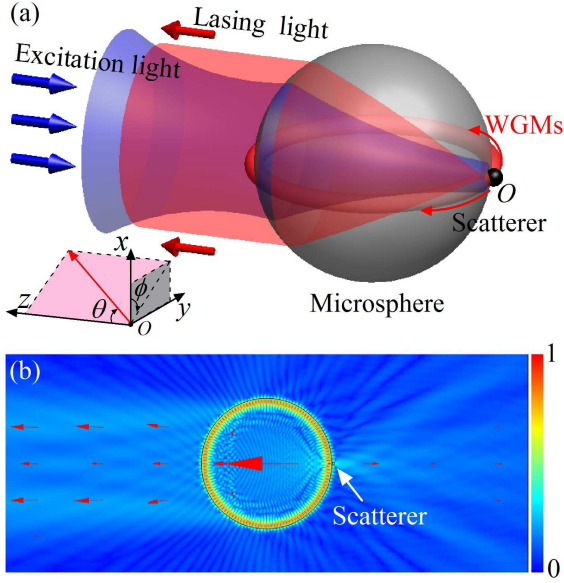


FIG. 1: (Color online) (a) Schematic illustration of the scatterer-microsphere coupling system (not to scale). Bottom left: the corresponding Cartesian and spherical coordinate systems, with θ the emitting angle and ϕ the azimuth angle. (b) Finite element simulations (COMSOL Multiphysics) of the directional emission mode. The color represents the square root of the electric field's absolute value $|E|^{1/2}$ (For clarity, we use $|E|^{1/2}$ in order to increase the contrast). The red arrows indicate the direction of power flow. In the simulation we use the radii $R = 10 \mu\text{m}$, $r_s = 200 \text{ nm}$, microsphere's refractive index $n = 1.7$.

The scattered lasing photons are collimated by the microsphere, giving rise to directional emission. In Fig. 1(b) the simulation results of wave approach is presented, demonstrating this directional emission mode. As a universal paradigmatic approach, the quantum treatment of Rayleigh scattering is widely used and well demonstrated [40, 42–45]. This quantum treatment is necessary because in such a scatterer-microsphere coupling system there exists a phenomenon similar with the Purcell effect, since the high state density of WGMs causes the enhanced scattering between the WGMs and the free-space reservoir modes [40, 42]. In the following we adopt this quantum approach to analyze the free-space excitation of WGMs and the free-space collection of scattered lasing modes, respectively.

III. FREE-SPACE EXCITATION

In this section, we develop the theoretical model to describe the scattering-induced coupling among the surrounding optical modes. By writing down the total Hamiltonian, we derive the equations of motion (quantum Langevin equations) for the free-space excitation process. Then we find analytical expressions for the coupling coefficients and the excitation efficiency. We also

address the focusing effect of the microsphere, which ensures efficient free-space excitation. At last specific examples are presented.

A. General Hamiltonian and Quantum Langevin equations

Under the rotating wave approximation, the total Hamiltonian for the free-space excitation process can be written as

$$H_1^{\text{tot}} = H_{\text{cav}}^{\text{f}} + H_{\text{in}}^{\text{f}} + H_{\text{res}}^{\text{f}} + H_{\text{cav-cav}}^{\text{i}} + H_{\text{cav-in}}^{\text{i}} + H_{\text{cav-res}}^{\text{i}}. \quad (1)$$

Here the superscript f (i) labels free (interaction) terms. The first three terms ($\hbar = 1$)

$$H_{\text{cav}}^{\text{f}} = \sum_m \omega_{1,m} a_m^\dagger a_m, \quad (2)$$

$$H_{\text{in}}^{\text{f}} = \int_{-\infty}^{+\infty} \omega b^\dagger(\omega) b(\omega) d\omega, \quad (3)$$

$$H_{\text{res}}^{\text{f}} = \sum_j \omega_j c_j^\dagger c_j, \quad (4)$$

describes the free radiation parts, where a_m , $b(\omega)$ and c_j denote annihilation operators of the m -th excitation WGM, the input modes and the j -th reservoir mode, with frequencies $\omega_{1,m}$, ω and ω_j , the commutation relation $[a_m, a_{m'}^\dagger] = \delta_{m,m'}$, $[b(\omega), b^\dagger(\omega')] = \delta(\omega - \omega')$, $[c_j, c_{j'}^\dagger] = \delta_{j,j'}$, respectively. For the WGMs in Eq. (2), we can neglect high order WGMs and focus on the fundamental WGMs, since they distribute around the equator of the microsphere, possess the minimum mode volume, the maximum Q factor, and are the typical lasing modes in actual experiments. Also, In the system described in Fig. 1(a), only transverse electric (TE) WGMs can be efficiently excited, and transverse magnetic (TM) WGMs can be safely neglected since the electric field of the TM WGMs are almost orthogonal to that of the input modes. Therefore, in Eq. (2) the summation index m runs through clockwise (CW) and counterclockwise (CCW) propagating fundamental WGMs, with a degenerate frequency denoted as $\omega_{1,m} \equiv \omega_1$.

The interaction terms of Eq. (1) are given by

$$H_{\text{cav-cav}}^{\text{i}} = \sum_{m,m'} g_{1,m,m'} a_m^\dagger a_{m'}, \quad (5)$$

$$H_{\text{cav-in}}^{\text{i}} = \sum_m \int_{-\infty}^{+\infty} [i g_{\text{in},m}(\omega) b^\dagger(\omega) a_m + \text{H.c.}] d\omega, \quad (6)$$

$$H_{\text{cav-res}}^{\text{i}} = \sum_{m,j} (g_{1,m,j} a_m^\dagger c_j + \text{H.c.}). \quad (7)$$

Here $H_{\text{cav-cav}}^{\text{i}}$ describes the interaction between the cavity modes, which results in the scattering into the same

($m = m'$) or the counterpropagating ($m \neq m'$) WGMs with amplitude coupling strengths $g_{1,m,m'}$; $H_{\text{cav-in}}^1$ represents the scattering between the input modes and the WGMs with coefficients $g_{\text{in},m}(\omega)$; $H_{\text{cav-res}}^1$ describes WGMs-reservoir scattering with coefficients $g_{1,m,j}$. Without loss of generality, in the following the coupling coefficients $g_{1,m,m'}$, $g_{\text{in},m}(\omega)$ and $g_{1,m,j}$ are assumed to be real for notational convenience. The degenerate CW and CCW WGMs have the same coupling strength in the scattering process, and thereby we denote $g_{1,m,m'} \equiv -g_1$, $g_{\text{in},m}(\omega) \equiv g_{\text{in}}(\omega)$ and $g_{1,m,j} \equiv g_{1,j}$. Note that in Eq. (1) we have neglected interacting terms like $H_{\text{in-in}}^1$, $H_{\text{res-res}}^1$, $H_{\text{in-res}}^1$, since they do not directly affect the cavity modes, and have minor effect on the system dynamics.

The eigenmodes of the system are the symmetric and antisymmetric standing modes, given by $a_{\pm} = (a_{\text{CW}} \pm a_{\text{CCW}})/\sqrt{2}$. Using the Heisenberg equations and the Markov approximation [46, 47], we obtain (see Appendix A for details)

$$\begin{aligned} \frac{da_+}{dt} = & -i(\omega_1 - 2g_1)a_+ - (\kappa_{\text{in}} + \kappa_{\text{R}})a_+ \\ & - \sqrt{2\kappa_{\text{in}}}b_{\text{in}} - \xi, \end{aligned} \quad (8)$$

where

$$\kappa_{\text{in}} = 2\pi g_{\text{in}}^2(\omega_1 - 2g_1), \quad (9)$$

$$\kappa_{\text{R}} = 2\pi \sum_j g_{1,j}^2 \delta(\omega - \omega_1 + 2g_1) \quad (10)$$

denotes the input-WGMs energy coupling strength and the decay of the WGMs induced by the Rayleigh scattering to the reservoir. b_{in} is the input field and ξ is the noise operator relate to the reservoir.

B. Scattering coefficients and excitation efficiency

In the full quantum theory, $g_{\text{in}}(\omega)$ and g_1 can be calculated as follows. The quantized electric field of the excitation WGMs at position \mathbf{R} is given by $\mathbf{E}_1(\mathbf{R}) = [E_1^{(+)}(\mathbf{R}) + E_1^{(-)}(\mathbf{R})]\hat{\mathbf{e}}_x$. Here $\hat{\mathbf{e}}_x$ is the unit vector along the x -axis direction,

$$E_1^{(+)}(\mathbf{R}) = \sqrt{\frac{\hbar\omega_1}{2\varepsilon_0\varepsilon_c V_1}} f_1(\mathbf{R})(a_{\text{CW}}e^{i\mathbf{k}_1 \cdot \mathbf{R}} + a_{\text{CCW}}e^{-i\mathbf{k}_1 \cdot \mathbf{R}}) \quad (11)$$

is the positive frequency component of the field and $E_1^{(-)}(\mathbf{R})$ is its adjoint; \mathbf{k}_1 is the wave vector of the CW mode; ε_0 is the dielectric permittivity of the vacuum and ε_c denotes the relative permittivity of the microsphere;

$$V_1 = \frac{\int \varepsilon(\mathbf{R}) |E_1(\mathbf{R})|^2 d\mathbf{R}^3}{\max[\varepsilon(\mathbf{R}) |E_1(\mathbf{R})|^2]} \quad (12)$$

is the mode volume of the WGMs, which can be calculated as [48]

$$V_1 = 3.4\pi^{\frac{3}{2}} \left(\frac{\lambda_1}{2\pi n} \right)^{\frac{7}{6}} R^{\frac{11}{6}}. \quad (13)$$

for a microsphere; $f_1(\mathbf{R}) = |E_1(\mathbf{R})/E_{1,\text{max}}|$ is the normalized field distribution function of the WGMs. The quantized electric field of the input beam at position (\mathbf{r}, z) is given by $\mathbf{E}_{\text{in}}(\mathbf{r}, z) = [E_{\text{in}}^{(+)}(\mathbf{r}, z) + E_{\text{in}}^{(-)}(\mathbf{r}, z)]\hat{\mathbf{e}}_x$, where $\mathbf{r} = (x\hat{\mathbf{e}}_x, y\hat{\mathbf{e}}_y)$. The positive frequency component reads

$$E_{\text{in}}^{(+)}(\mathbf{r}, z) = -i \sum_k \sqrt{\frac{\hbar\omega_k}{2\varepsilon_0 V_k}} f_{\text{in},k}(\mathbf{r}) b_k e^{ikz}, \quad (14)$$

where ε_b denotes the relative permittivity of the surrounding medium, b_k is the annihilation operator of the k -th mode, V_k ($f_{\text{in},k}(\mathbf{r})$) is the corresponding mode volume (field distribution function). The expression can be rewritten as an integral form [47]

$$E_{\text{in}}^{(+)}(\mathbf{r}, z) = -i \int d\omega \sqrt{\frac{\hbar\omega}{4\pi\varepsilon_0 c A(z)}} f_{\text{in}}(\mathbf{r}) b(\omega) e^{ikz}. \quad (15)$$

Here c is the speed of light in vacuum; $A(z)$ is the mode area on $x-y$ plane, given by

$$A(z) = \frac{\int \varepsilon(\mathbf{r}) |E_{\text{in}}(\mathbf{r})|^2 d\mathbf{r}^2}{\max[\varepsilon(\mathbf{r}) |E_{\text{in}}(\mathbf{r})|^2]}. \quad (16)$$

For Gaussian beam $A(z) = \iint_{-\infty}^{\infty} e^{-2(x^2+y^2)/w(z)^2} dx dy = \pi w(z)^2/2$, where $w(z)$ is the spot radius at z . The quantized electric field of the reservoir is given by $\mathbf{E}_j(\mathbf{R}) = [E_j^{(+)}(\mathbf{R}) + E_j^{(-)}(\mathbf{R})]\hat{\mathbf{e}}_j$, where

$$E_j^{(+)}(\mathbf{R}) = \sqrt{\frac{\hbar\omega_j}{2\varepsilon_0 V_j}} a_j e^{i\mathbf{k}_j \cdot \mathbf{R}}, \quad (17)$$

with V_j , \mathbf{k}_j and $\hat{\mathbf{e}}_j$ being the mode volume, wave vector and the unit vector along polarization direction of the j -th reservoir mode.

The interaction via scattering yields the Hamiltonian [40, 42, 43, 45]

$$H^{\text{i}} = -\frac{1}{2} \mathbf{p}_s \cdot \mathbf{E}_s, \quad (18)$$

where

$$\mathbf{E}_s = \mathbf{E}_1(\mathbf{0}) + \mathbf{E}_{\text{in}}(\mathbf{0}, 0) + \mathbf{E}_j(\mathbf{0}), \quad (19)$$

$$\mathbf{p}_s = \varepsilon_0 \alpha \mathbf{E}_s \quad (20)$$

are the total electric field at the position of the scatterer (the origin O of the coordinate system) and the total polarization of the scatterer; $\alpha = 4\pi r_s^3(\varepsilon_s - 1)/(\varepsilon_s + 2)$ is the polarizability of the spherical scatterer with ε_s being its relative permittivity. Note that for Gaussian beam the maximum electric field is at the center of the beam, yielding $f_{\text{in}}(\mathbf{0}) = 1$. Using the above equations, we obtain

the coupling coefficients as

$$g_1 = \frac{\alpha\omega_1 f_1^2(\mathbf{0})}{2\epsilon_c V_1}, \quad (21)$$

$$g_{\text{in}}(\omega) = -\frac{1}{2}\alpha f_1(\mathbf{0})\sqrt{\frac{\omega_1\omega}{2\pi\epsilon_c c V_1 A_s}}, \quad (22)$$

$$g_{1,j} = -\frac{1}{2}\alpha f_c(\mathbf{0})\sqrt{\frac{\omega_1\omega_j}{\epsilon_c V_1 V_j}}(\hat{\mathbf{e}}_x \cdot \hat{\mathbf{e}}_j), \quad (23)$$

and thereby the in-coupling strength can be obtained as

$$\kappa_{\text{in}} = \frac{\alpha^2 f_1^2(\mathbf{0})\omega_1(\omega_1 - 2g_1)}{4\epsilon_c c V_1 A_s}, \quad (24)$$

$$\kappa_{\text{R}} = \frac{(n^5 + 1)\alpha^2\omega_1(\omega_1 - 2g_1)^3 f_1^2(\mathbf{0})}{12\pi c^3 \epsilon_c V_1}, \quad (25)$$

where $A_s = \pi w_s^2/2$, with w_s being the spot radius at $z = 0$ plane (where the scatterer is located at).

The excitation efficiency can be defined as $\eta = 1 - T_{\text{min}}$, where T_{min} is the minimum value of the transmission. From Eq. (8), we obtain (see Appendix B for details)

$$\eta = \frac{4\kappa_{\text{in}}(\kappa_0 + \kappa_{\text{R}})}{(\kappa_0 + \kappa_{\text{in}} + \kappa_{\text{R}})^2}. \quad (26)$$

C. Focusing effect of the microsphere and specific examples

To realize efficient coupling, the input beam should be focused into a small spot on the scatterer, since κ_{in} is in inverse proportion to the mode area A_s , as shown in Eq. (24). In fact, the microsphere is a natural optical lens which possesses ultrashort focal length, capable of focusing the light spot significantly. Numerical simulation shows that circular dielectric cylinders illuminated by a plane wave can generate nanojets with waists smaller than the diffraction limit [49, 50]. Here we use Gaussian beam input and analytically treat the problem using Gaussian beam transform laws. The sphere can be viewed as a thick lens, with the focal length

$$F = \frac{nR}{2(n-1)}, \quad (27)$$

where n is the relative refractive index between the sphere and the environment ($n = \sqrt{\epsilon_c}$). As depicted in Fig. 2(a), the input light is assumed to be Gaussian beam with a waist radius w_0 ($w_0 < R$), and the distance between the beam waist and the center of the microsphere is s . After being focused by the sphere, the beam waist becomes

$$w'_0 = \frac{Fw_0}{\sqrt{(s-F)^2 + z_{\text{R}}^2}}, \quad (28)$$

with its distance to the center of the microsphere given by

$$s' = \frac{s(s-F) + z_{\text{R}}^2 F}{(s-F)^2 + z_{\text{R}}^2}, \quad (29)$$

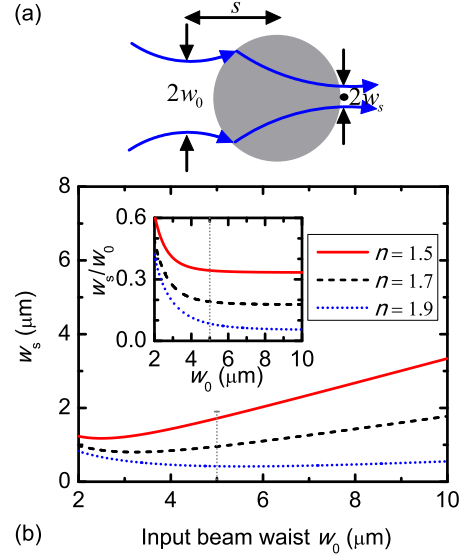


FIG. 2: (Color online) (a) Illustration of the microsphere-induced focusing effect, with w_0 being the input beam waist and w_s being the resulting spot radius at $z = 0$ plane, after being focused by the microsphere. (b) w_s vs. w_0 for different cavity refractive index n . Inset: spot radius minification w_s/w_0 as a function of w_0 . The dotted vertical lines indicate $w_0 = 5 \mu\text{m}$. Here the microsphere's radius $R = 10 \mu\text{m}$.

where $z_{\text{R}} \equiv \pi w_0^2 n / \lambda$ is the Rayleigh range. Then the spot radius at $z = 0$ plane is

$$w_s = w'_0 \sqrt{1 + \left(\frac{s' - R}{z'_{\text{R}}}\right)^2}, \quad (30)$$

with $z'_{\text{R}} \equiv \pi w_0'^2 n / \lambda$.

In Fig. 2(b) we give a specific example, where $R = 10 \mu\text{m}$, $s = 0$; for dopant Er^{3+} , the excitation wavelength $\lambda_1 = 977 \text{ nm}$ (lasing wavelength $\lambda_2 = 1550 \text{ nm}$). We plot the resulting spot radius w_s as a function of the input beam waist w_0 for different refractive index $n = 1.5, 1.7, 1.9$. It is shown that for relatively large input beam waist, the microsphere is able to focus the beam intensely, especially when n approaches 2. For $F \ll z_{\text{R}}$, i. e., $w_0^2 \gg \lambda R / [2\pi(n-1)]$, we obtain $w_s \simeq (|2-n|/n)w_0$, which indicates a $|2-n|/n$ times decrease of the spot radius, as further plotted in the inset of Fig. 2(b). This is consistent with the ray optics predictions. Therefore, it is of great advantage to make use of the cavity itself as a micro-sized lens.

Now we study the in-coupling strength κ_{in} and Rayleigh scattering induced decay κ_{R} as a function of the scatterer's radius r_s as shown in Fig. 3(a)-(b), where we have set $w_0 = 5 \mu\text{m}$, and other parameters: $\epsilon_s = 12$ (silicon), $f_1(\mathbf{0}) = 0.4$ (We will use there parameters unless specified). The free-space excitation efficiency for different radii of both the scatterer and the microsphere are presented in Fig. 3(c)-(d), which shows more than 10% excitation efficiency can be obtained for suitable param-

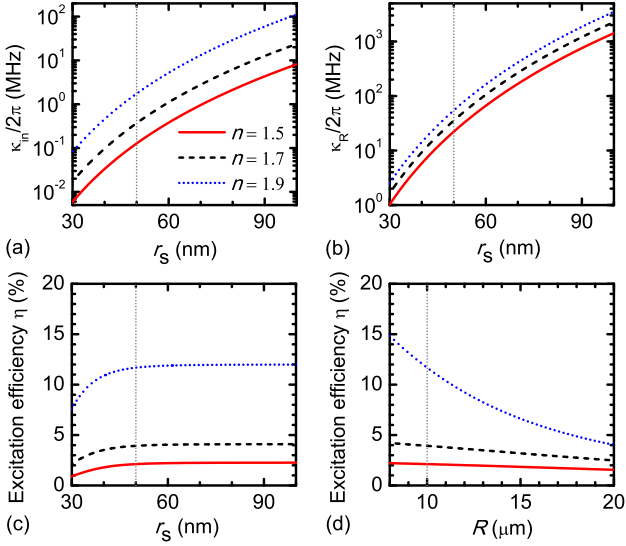


FIG. 3: (Color online) (a)-(b) In-coupling strength κ_{in} and Rayleigh scattering induced decay κ_R as a function of the scatterer's radius r_s for different cavity refractive index n . (c)-(d) Excitation efficiency η as a function of r_s and R . In (a)-(c), we use $R = 10 \mu\text{m}$, corresponding to the dotted vertical line in (d); in (d), $r_s = 50 \mu\text{m}$, corresponding to the dotted vertical line in (a)-(c).

ters. In Fig. 3(c), for small scatterer, the cavity intrinsic decay κ_0 dominates over κ_{in} and κ_R , which results in low excitation efficiency. For large scatterer, κ_0 can be neglected compared with κ_R , yielding a constant excitation efficiency decided by κ_{in} and κ_R . In Fig. 3(d), smaller microspheres possess smaller mode volumes, resulting in larger κ_{in} and κ_R , and thereby larger excitation coefficient. In addition, smaller microspheres have stronger focusing effects, leading to larger κ_{in} . To obtain a better excitation efficiency, we should increase κ_{in} and meanwhile decrease κ_0 and κ_R . This can be realized by using smaller input beam waist and by using microcavity with proper refractive index, which lead to small mode area A_s , as discussed above.

IV. FREE-SPACE COLLECTION

For free-space collection process, the Hamiltonian is similar with that of free-space excitation process (Eq. (1)) by dropping the terms containing the input modes. Mention that the energy scattered from the lasing WGMs into the reservoir modes is just the output of laser emission. Quite different from the ordinary case in which this kind of scattering leads to pure damping and is always harmful, here it is a kind of useful resource and plays a key role in obtaining directional laser emission. This scattering offers an interface between the WGMs inside the microcavity and the optical modes outside the cavity, where we use the coefficient κ_{out} to denote the out-coupling strength. Following the calculation of scattering

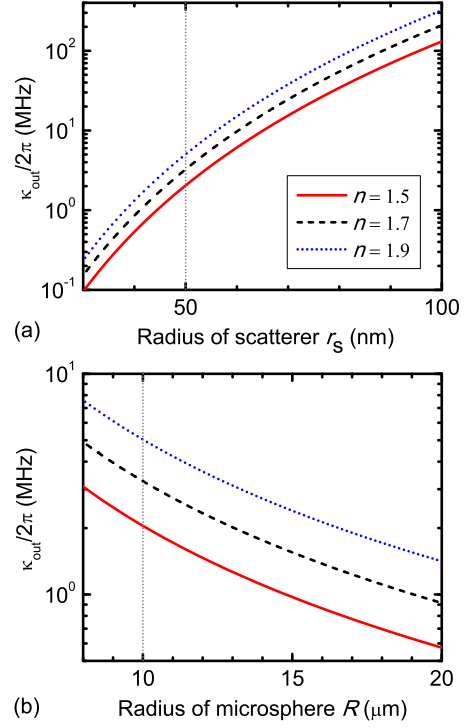


FIG. 4: (Color online) Out-coupling strength κ_{out} as a functions of the scatterer's radius r_s (a) and microsphere's radius R (b) for different cavity refractive index n .

coefficients in the above section, we obtain

$$\kappa_{out} = 2\pi \sum_j g_{2,j}^2 \delta(\omega - \omega_2 + 2g_2) \quad (31)$$

$$= \frac{(n^5 + 1)\alpha^2 \omega_2 (\omega_2 - 2g_2)^3 f_2^2(\mathbf{0})}{12\pi c^3 \epsilon_c V_2}, \quad (32)$$

where

$$g_2 = \frac{\alpha \omega_2 f_2^2(\mathbf{0})}{2\epsilon_c V_2}, \quad (33)$$

$$g_{2,j} = -\frac{1}{2}\alpha f_2(\mathbf{0}) \sqrt{\frac{\omega_2 \omega_j}{\epsilon_c V_2 V_j}} (\hat{\mathbf{e}}_x \cdot \hat{\mathbf{e}}_j), \quad (34)$$

and V_2 ($f_2(\mathbf{0})$) is the mode volume (field distribution function) of the lasing WGMs.

Figure 4 plots κ_{out} as a function of the radii of the scatterer and the microsphere. For $r_s = 50 \text{ nm}$ and $R = 10 \mu\text{m}$, κ_{out} is several mega Hertz, which corresponds to $Q_{out} = \omega_2/\kappa_{out} \sim 10^8$. Therefore, the high- Q properties of the lasing modes can be maintained.

In the following we analyze the emission directionality originating from Rayleigh scattering and collimating effect of the microsphere. Finally the emission directionality and energy collection ratio for various parameters are present.

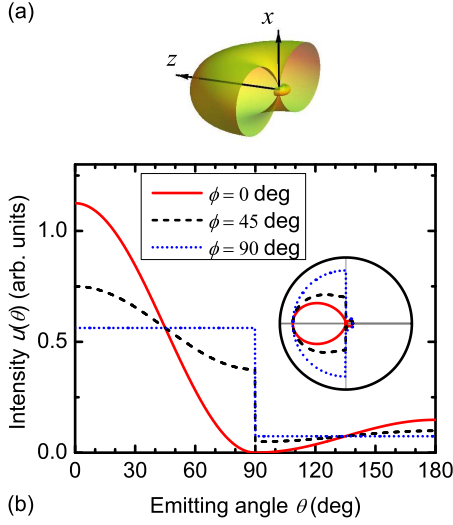


FIG. 5: (Color online) (a) Spherical plot of $u(\theta, \phi)$. (b) $u(\theta, \phi)$ vs. θ for various ϕ . Inset: The corresponding polar plot of $u(\theta, \phi)$. Here we use $n = 1.5$.

A. Scattering directionality

The factor $\hat{\mathbf{e}}_x \cdot \hat{\mathbf{e}}_j$ in Eq. (34) indicates that $g_{2,j}$ depends on the direction, resulting the direction-dependent out-coupling coefficient $\kappa(\theta, \phi)$, which satisfies $\kappa_{\text{out}} = \iint \kappa(\theta, \phi) d\Omega$, with Ω being the solid angle and $d\Omega = \sin \theta d\theta d\phi$. After normalization, we can define $u(\theta, \phi) = \kappa(\theta, \phi) / \kappa_{\text{out}}$, which can be calculated as

$$u(\theta, \phi) = \begin{cases} \frac{3n^5(1-\sin^2 \theta \cos^2 \phi)}{4\pi(n^5+1)}, & 0^\circ \leq \theta < 180^\circ, \\ \frac{3(1-\sin^2 \theta \cos^2 \phi)}{4\pi(n^5+1)}, & 180^\circ \leq \theta < 360^\circ. \end{cases} \quad (35)$$

The normalized out-coupling coefficient $u(\theta, \phi)$ represents the angular distribution of output energy. In Fig. 5(a) we present $u(\theta, \phi)$ for given azimuth angle $\phi = 0^\circ, 45^\circ, 90^\circ$, respectively. Note that for $0^\circ \leq \theta < 180^\circ$ the environment is dielectric cavity with permittivity of ϵ_c , while for $180^\circ \leq \theta < 360^\circ$ that is vacuum with permittivity of 1. As shown in Fig. 5, the light tends to be scattered to z axis ($\theta = 0^\circ, 180^\circ$), but the scattering along $+z$ axis is much stronger due to the asymmetry environment. Note that for $\phi = 90^\circ$, the scattering is uniform in the same environment, since in this case the scattered light has the same polarization with the WGMs.

B. Collimating effect of the microsphere

Although the scattered light trends to propagate along z axis, the divergency angle is too wide. To obtain better directionality, once again we can make use of the microsphere itself, which behaves as a thick lens. As depicted in the inset of Fig. 6(b), the emitted light for $0^\circ \leq \theta < (180^\circ/\pi) \arcsin(1/n)$ (the critical angles of total reflection) passes through the microsphere, and finally

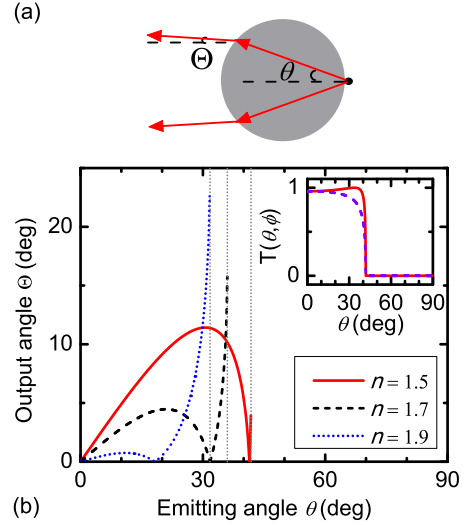


FIG. 6: (Color online) (a) Illustration of the microsphere-induced collimating effect. (b) Θ vs. θ for $n = 1.5, 1.7, 1.9$. The dotted vertical lines correspond to the critical angles of total reflection for $n = 1.5, 1.7, 1.9$ (from right to left). Inset: Transmission as a function of θ for $\phi = 0^\circ$ (solid), 90° (dashed), here $n = 1.5$.

yields the output angle Θ , given by

$$\Theta = f(\theta) = |2\theta - \arcsin(n \sin \theta)|. \quad (36)$$

Note that for $(180^\circ/\pi) \arcsin(1/n) \leq \theta < 90^\circ$, the light is totally reflected on the microsphere surface. From Fig. 6(b) we can see that the output angle Θ has a much small divergence than the emitting angle θ , which stems from the collimating effect of the microsphere.

The output energy density function can be obtained as

$$p(\Theta, \phi) = \sum T(f^{-1}(\Theta), \phi) u(f^{-1}(\Theta), \phi) \frac{df^{-1}(\Theta)}{d\Theta}, \quad (37)$$

where

$$T(\theta, \phi) = T_p(\theta, \phi) \cos^2 \phi + T_s(\theta, \phi) \sin^2 \phi; \quad (38)$$

T_p (T_s) is the transmission for p-polarization (s-polarization) component, calculated from Fresnel formula; $\theta = f^{-1}(\Theta)$ is the inverse function of $f(\theta)$, which is a multiple valued function, and \sum means the summation over each section of the multiple valued function. Note that $p(\Theta, \phi)$ has singularities, thus the full-width-of-half-maximum definition of the divergence angle fails. To quantify the emission directionality, we define a half-energy angle $\Theta_{1/2}$, given by $P(\Theta_{1/2}, \phi) = 1/2$, where

$$P(\Theta, \phi) = \int_0^\Theta p(\Theta', \phi) d\Theta' \quad (39)$$

is the energy ratio (energy distribution function), representing how much energy distributes in the interval $[0, \Theta]$. This half-energy angle represents that the output angle of half light is smaller than $\Theta_{1/2}$.

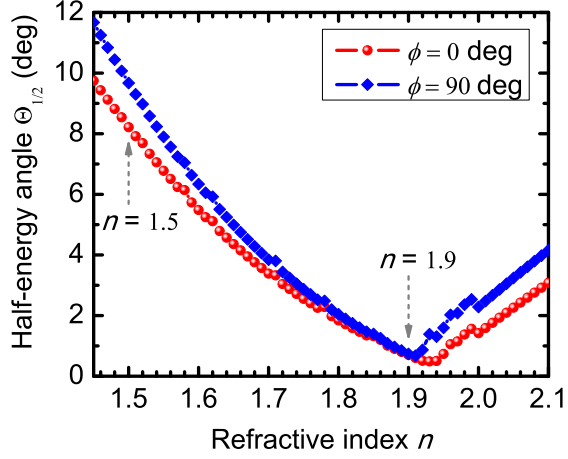


FIG. 7: (Color online) (a) Half energy angle $\Theta_{1/2}$ vs. n for $\phi = 0^\circ, 90^\circ$.

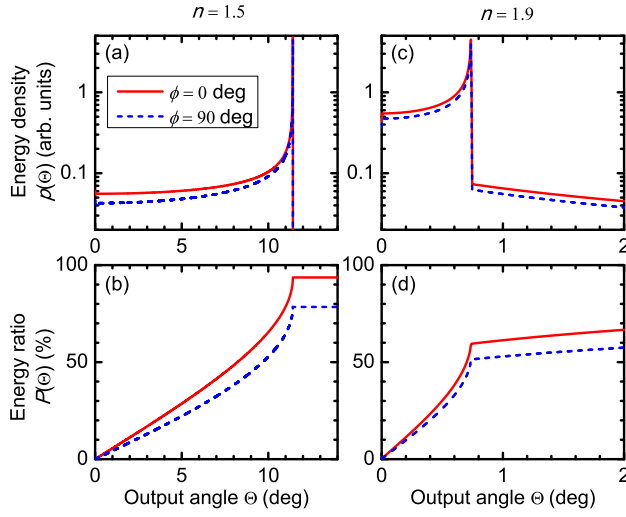


FIG. 8: (Color online) Energy density $p(\Theta)$ and energy ratio $P(\Theta)$ as functions of Θ different n and ϕ . (a)-(b): $n = 1.5$; (d)-(e): $n = 1.9$.

In Fig. 7 we plot the half-energy angle as a function of the refractive index for $\phi = 0^\circ$ and 90° . Note that these two cases set the lower and upper bounds, as inferred from the emission pattern in Fig. 5(a). Remarkably, $\Theta_{1/2}$ can be less than 1° (for refractive index around 1.9), which indicates much better directionality than previous predictions based on other mechanisms, to the best of our knowledge.

As two specific cases, the energy density function $p(\Theta, \phi)$ and the energy ratio $P(\Theta, \phi)$ for $n = 1.5$ and 1.9 are plotted in Fig. 8(b)-(e). For $n = 1.5$, more than 80% emission energy can be collected within $\Theta \simeq 11^\circ$. For $n = 1.9$, very good directionality can be obtained, with over 50% collection efficiency for $\Theta \leq 0.7^\circ$.

For widely used microcavities with the refractive index not equal to 1.9 (e.g., Silica, Calcium Fluoride, Lithium Niobate), the optimal emission directionality can be obtained by optimizing the shape of the microcavity (e.g., using deformed cavities) and the position of the scatterer (e.g. embedding the scatterer inside the microcavity). Note that this optimal refractive index is irrelevant with the size, shape and material of the scatterer.

V. CONCLUSION

In summary, based on cavity QED approach, we analytically investigate the microsphere-scatterer coupling system in which the high-Q WGMs can be efficiently excited through free space and the resulting laser is capable of emitting with high directionality. In this system, a subwavelength scatterer placed in the vicinity of the microsphere serves as an interface between the input light, the WGMs and the output light. We take advantage of the microsphere itself to focus the input beam with small spot area, and collimate the output beam with ultra-small divergence angle. Our results show that the high-Q WGMs can be excited with efficiency larger than 10%. More importantly, the half-energy angle of the output light can be as narrow as 0.7° , which is a great improvement over the 2D microcavity lasers [38, 39]. This holds great potential for novel micro-sized laser sources and has broad applications in Micro/Nano photonics.

Acknowledgments

This work was supported by the NSFC (Grants No. 10821062, No. 11004003, and No. 11023003) and the 973 program (Grant No. 2007CB307001).

Appendix A: Derivation of Quantum Langevin equations

Starting from the total Hamiltonian H_1^{tot} (Eq. (1)), the Heisenberg equations of motion can be derived as

$$\frac{da_m}{dt} = -i\omega_1 a_m - \int_{-\infty}^{+\infty} g_{\text{in}}(\omega) b(\omega) d\omega + ig_1 \sum_{m'} a_{m'} - i \sum_j g_{1,j} c_j, \quad (\text{A1})$$

$$\frac{db(\omega)}{dt} = -i\omega b(\omega) + g_{\text{in}}(\omega) \sum_m a_m, \quad (\text{A2})$$

$$\frac{dc_j}{dt} = -i\omega_j c_j - ig_{1,j} \sum_m a_m. \quad (\text{A3})$$

The eigenmodes of the system are the symmetric and antisymmetric standing modes, given by $a_{\pm} = (a_{\text{CW}} \pm$

$a_{\text{CCW}})/\sqrt{2}$. Then the above equations can be rewritten as

$$\frac{da_+}{dt} = -i\omega_1 a_+ - \sqrt{2} \int_{-\infty}^{+\infty} g_{\text{in}}(\omega) b(\omega) d\omega + i2g_1 a_+ - i\sqrt{2} \sum_j g_{1,j} c_j, \quad (\text{A4})$$

$$\frac{da_-}{dt} = -i\omega_c a_-, \quad (\text{A5})$$

$$\frac{db(\omega)}{dt} = -i\omega b(\omega) + \sqrt{2} g_{\text{in}}(\omega) a_+, \quad (\text{A6})$$

$$\frac{dc_j}{dt} = -i\omega_j c_j - i\sqrt{2} g_{1,j} a_+. \quad (\text{A7})$$

Formal integrations of Eq. (A6) and (A7) yield

$$b(\omega) = e^{-i\omega(t-t_0)} b_0(\omega) + \sqrt{2} g_{\text{in}}(\omega) \int_{t_0}^t e^{-i\omega(t-t')} a_+(t') dt', \quad (\text{A8})$$

$$c_j = e^{-i\omega_j(t-t_0)} c_{j,0} - i\sqrt{2} g_{1,j} \int_{t_0}^t e^{-i\omega_j(t-t')} a_+(t') dt', \quad (\text{A9})$$

where $b_0(\omega)$, $c_{j,0}$ denotes the value of $b(\omega)$, c_j at $t = t_0$, respectively. In both equations the first terms represent the free evolution of the modes while the second terms

arise from the interaction with the WGMs.

Substituting the solutions into Eq. (A4), we finally obtain

$$\frac{da_+}{dt} = -i(\omega_1 - 2g_1) a_+ - (\kappa_{\text{in}} + \kappa_{\text{R}}) a_+ - \sqrt{2\kappa_{\text{in}}} b_{\text{in}} - \xi, \quad (\text{A10})$$

where

$$\kappa_{\text{in}} = 2\pi g_{\text{in}}^2 (\omega_1 - 2g_1) \quad (\text{A11})$$

represents the input-WGMs energy coupling strength,

$$b_{\text{in}} = \frac{1}{\sqrt{2\pi}} \int_{-\infty}^{+\infty} b_0(\omega) e^{-i\omega(t-t_0)} d\omega \quad (\text{A12})$$

describes the input field,

$$\kappa_R = 2\pi \sum_j g_{1,j}^2 \delta(\omega - \omega_1 + 2g_1) \quad (\text{A13})$$

denotes the damping of the WGMs induced by the scattering to the reservoir,

$$\xi = i\sqrt{2} \sum_j g_{1,j} e^{-i\omega_j(t-t_0)} c_{j,0} \quad (\text{A14})$$

is the noise operator relate to the reservoir. In deriving Eq. (A10), we have used the Markov approximation [46].

Appendix B: Derivation of excitation efficiency

Taking the intrinsic decay rate κ_0 of the WGMs into account, and using the input-output relation [46, 47]

$$b_{\text{out}} = b_{\text{in}} + \sqrt{2\kappa_{\text{in}}} a_+, \quad (\text{B1})$$

we obtain

$$b_{\text{out}} = b_{\text{in}} + \frac{2\kappa_{\text{in}} b_{\text{in}} + \sqrt{2\kappa_{\text{in}}} \xi}{i(\omega - \omega_1 + 2g_1) - (\frac{\kappa_0}{2} + \kappa_{\text{in}} + \kappa_R)}. \quad (\text{B2})$$

Then the transmission can be obtained as $T = \langle b_{\text{out}}^\dagger b_{\text{out}} \rangle / \langle b_{\text{in}}^\dagger b_{\text{in}} \rangle$. For optical frequency, room temperature, the initial states of the reservoir modes are almost all vacuum states. Thus the expectation values of the noise operators can be neglected. Therefore, we obtain the minimum value of the transmission

$$T_{\text{min}} = \left(\frac{2\kappa_{\text{in}} - \kappa_0 - 2\kappa_R}{2\kappa_{\text{in}} + \kappa_0 + 2\kappa_R} \right)^2. \quad (\text{B3})$$

Thus the excitation efficiency $\eta = 1 - T_{\text{min}}$ can be obtained as

$$\eta = \frac{4\kappa_{\text{in}}(\kappa_0 + 2\kappa_R)}{(\kappa_0 + 2\kappa_{\text{in}} + 2\kappa_R)^2}. \quad (\text{B4})$$

-
- [1] K. J. Vahala, *Nature* **424**, 839 (2003).
 - [2] V. S. Ilchenko and A. B. Matsko, *IEEE J. Sel. Top. Quantum Electron.* **12**, 3 (2006).
 - [3] A. Chiasera, Y. Dumeige, P. Féron, M. Ferrari, Y. Jestin, G. N. Conti, S. Pelli, S. Soria, G. C. Righini, *Laser & Photon. Rev.* **4**, 457 (2010).
 - [4] J. Ward and O. Benson, *Laser & Photon. Rev.* **5**, 553 (2011).
 - [5] S. L. McCall, A. F. J. Levi, R. E. Slusher, S. J. Pearton, and R. A. Logan, *Appl. Phys. Lett.* **60**, 289 (1992).
 - [6] J. C. Knight, G. Cheung, F. Jacques, and T.A. Birks, *Opt. Lett.* **22**, 1129 (1997).
 - [7] M. Cai, O. Painter, and K. J. Vahala, *Phys. Rev. Lett.* **85**, 74 (2000).
 - [8] S. M. Spillane, T. J. Kippenberg, O. J. Painter, and K. J. Vahala, *Phys. Rev. Lett.* **91**, 043902 (2003).
 - [9] Y.-S. Park, A. K. Cook, and H. Wang, *Nano Lett.* **6**, 2075 (2006).
 - [10] Y.-S. Park and H. Wang, *Nat. Phys.* **5**, 489 (2009).
 - [11] J. Yang, S.-B. Lee, S. Moon, S.-Y. Lee, S. W. Kim, T. T. Dao, J.-H. Lee, and K. An, *Phys. Rev. Lett.* **104**, 243601 (2010).
 - [12] V. S. Ilchenko, A. A. Savchenkov, A. B. Matsko, and L. Maleki, *Phys. Rev. Lett.* **92**, 043903 (2004).
 - [13] I. S. Grudinin, V. S. Ilchenko, and L. Maleki, *Phys. Rev. A* **74**, 063806 (2006).
 - [14] A. F. J. Levi, R. E. Slusher, S. L. McCall, J. L. J. Glass, S. J. Pearton, and R. A. Logan, *Appl. Phys. Lett.* **62**, 561 (1993).
 - [15] A. Mekis, J. U. Nöckel, G. Chen, A. D. Stone, and R. K. Chang, *Phys. Rev. Lett.* **75**, 2682 (1995).
 - [16] J. U. Nöckel and A. D. Stone, *Nature* **385**, 45 (1997).
 - [17] C. Gmachl, F. Capasso, E. E. Narimanov, J. U. Nöckel, A. D. Stone, J. Faist, D. L. Sivco, A. Y. Cho, *Science* **280**, 1556 (1998).
 - [18] S.-B. Lee, J.-H. Lee, J.-S. Chang, H.-J. Moon, S. W. Kim, and K. An, *Phys. Rev. Lett.* **88**, 033903 (2002).
 - [19] S. Lacey, H. Wang, D. H. Foster, and J. U. Nöckel, *Phys. Rev. Lett.* **91**, 033902 (2003).
 - [20] T. Harayama, T. Fukushima, S. Sunada, and K. S. Ikeda, *Phys. Rev. Lett.* **91**, 073903 (2003).
 - [21] G. D. Chern, H. E. Tureci, A. Douglas Stone, R. K. Chang, M. Kneissl, and N. M. Johnson, *Appl. Phys. Lett.* **83**, 1710 (2003).
 - [22] T. Fukushima, T. Tanaka, and T. Harayama, *Appl. Phys. Lett.* **86**, 171103 (2005).
 - [23] W. Fang, A. Yamilov, and H. Cao, *Phys. Rev. A* **72**, 023815 (2005).
 - [24] M. Lebental, J. S. Lauret, R. Hierle, and J. Zyss, *Appl. Phys. Lett.* **88**, 031108 (2006).
 - [25] R. Schäfer, U. Kuhl, and H.-J. Stöckmann, *New J. Phys.* **8**, 46 (2006).
 - [26] Y.-F. Xiao, C.-H. Dong, C.-L. Zou, Z.-F. Han, L. Yang and G.-C. Guo, *Opt. Lett.* **34**, 509 (2009).
 - [27] C.-L. Zou, F.-W. Sun, C.-H. Dong, X.-W. Wu, J.-M. Cui, Y. Yang, G.-C. Guo, and Z.-F. Han, *arXiv:0908.3531*.
 - [28] S. Shinohara, T. Harayama, T. Fukushima, M. Hentschel, T. Sasaki, and E. E. Narimanov, *Phys. Rev. Lett.* **104**, 163902 (2010).
 - [29] F.-J. Shu, C.-L. Zou, F.-W. Sun, and Y.-F. Xiao, *Phys. Rev. A* **83**, 053835 (2011).
 - [30] T. Harayama and S. Shinohara, *Laser Photon. Rev.* **5**, 247 (2011).
 - [31] J. Wiersig and M. Hentschel, *Phys. Rev. Lett.* **100**, 033901 (2008).
 - [32] C. Yan, Q. J. Wang, L. Diehl, M. Hentschel, J. Wiersig, N. Yu, C. Pflüg, F. Capasso, M. A. Belkin, T. Edamura, M. Yamanishi, and H. Kan, *Appl. Phys. Lett.* **94**, 251101 (2009).

- (2009).
- [33] C.-H. Yi, M.-W. Kim, and C.-M. Kim, Appl. Phys. Lett. **95**, 141107 (2009).
 - [34] Q. H. Song, L. Ge, A. D. Stone, H. Cao, J. Wiersig, J. B. Shim, J. Unterhinninghofen, W. Fang, and G. S. Solomon, Phys. Rev. Lett. **105**, 103902 (2010).
 - [35] V. M. Apalkov and M. E. Raikh, Phys. Rev. B **70**, 195317 (2004).
 - [36] J. Wierisig and M. Hentschel, Phys. Rev. A **73**, 031802 (2006).
 - [37] C. P. Dettmann, G. V. Morozov, M. Sieber, and H. Waalkens, Phys. Rev. A **80**, 063813 (2009).
 - [38] Q. J. Wang, C. Yan, N. Yu, J. Unterhinninghofen, J. Wiersig, C. Pflügl, L. Diehl, T. Edamura, M. Yamanishi, H. Kan, and F. Capasso, P. Natl. Acad. Sci. **107**, 22407 (2010).
 - [39] Q. H. Song and H. Cao, Opt. Lett. **36**, 103 (2011).
 - [40] A. Mazzei, S. Götzinger, L. de S. Menezes, G. Zumofen, O. Benson and V. Sandoghdar, Phys. Rev. Lett. **99**, 173603 (2007).
 - [41] L. Deych and J. Rubin, Phys. Rev. A **80**, 061805(R) (2009).
 - [42] T. J. Kippenberg, A. L. Tchebotareva, J. Kalkman, A. Polman, and K. J. Vahala, Phys. Rev. Lett. **103**, 027406 (2009).
 - [43] J. Zhu, S. K. Ozdemir, Y.-F. Xiao, L. Li, L. He, D.-R. Chen, and L. Yang, Nat. Photon **4**, 46 (2010).
 - [44] X. Yi, Y.-F. Xiao, Y.-C. Liu, B.-B. Li, Y.-L. Chen, Y. Li, and Q. Gong, Phys. Rev. A **83**, 023803 (2011).
 - [45] Y.-C. Liu, Y.-F. Xiao, B.-B. Li, X.-F. Jiang, Y. Li, and Q. Gong, Phys. Rev. A **84**, 011805(R) (2011).
 - [46] C. W. Gardiner and P. Zoller, *Quantum Noise*, 3rd ed. (Springer, Berlin, 2004).
 - [47] D. F. Walls and G. J. Milburn, *Quantum Optics*, 2nd ed. (Springer, Berlin, 2008).
 - [48] V. B. Braginsky, M. L. Gorodetsky, and V. S. Ilchenko, Phys. Lett. A **137**, 393 (1989).
 - [49] Z. G. Chen, A. Taflowe, and V. Beckman, Opt. Express **12**, 1214 (2004).
 - [50] X. Li, Z. G. Chen, A. Taflowe, and V. Backman, Opt. Express **13**, 526 (2005).